coatings

MDPI

Article

Preparation of Highly Durable Columnar Suspension Plasma Spray (SPS) Coatings by Pre-Oxidation of the CoNiCrAlY Bondcoat

Jana Joeris [1,*], Walter Sebastian Scheld [1], Sven Uhlenbruck [1], Yoo Jung Sohn [1], Doris Sebold [1], Olivier Guillon [1,2] and Robert Vaßen [1,3]

[1] Forschungszentrum Jülich GmbH, Institute of Energy and Climate Research, Materials Synthesis and Processing (IEK-1), 52425 Jülich, Germany
[2] Jülich Aachen Research Alliance (JARA-Energy), 52425 Jülich, Germany
[3] Institut für Werkstoffe, Ruhr-Universität Bochum, 44801 Bochum, Germany
* Correspondence: j.joeris@fz-juelich.de

Abstract: Columnar structured thermal barrier coatings (TBCs) have been intensively investigated due to their potential to enhance the durability and reliability of gas turbine engine components. These coatings consist of vertically aligned columns that provide excellent resistance to thermal cycling. In this study, the lifetime of columnar suspension-plasma-sprayed (SPS) TBCs was evaluated using burner rig tests. The tests were carried out under high-temperature conditions. Significantly, the pre-oxidation of the bondcoat during diffusion bonding treatment was found to have a substantial impact on the performance of the SPS TBCs. The optimized treatment resulted in columnar SPS TBCs demonstrating excellent thermal stability and resistance under the test conditions. The lifetime of the coatings was significantly extended compared to conventional TBCs by pre-oxidation of the CoNiCrAlY bondcoat in argon, which suggests that columnar SPS TBCs have great potential for use in gas turbine engines.

Keywords: thermal barrier coating (TBC); yttria-stabilized zirconia (YSZ); axial suspension plasma spraying (SPS); columnar coatings; vacuum plasma spraying (VPS); thermally grown oxide; thermal cycling; phase characterization; oxide-dispersion-strengthened bondcoat

check for updates

Citation: Joeris, J.; Scheld, W.S.; Uhlenbruck, S.; Sohn, Y.J.; Sebold, D.; Guillon, O.; Vaßen, R. Preparation of Highly Durable Columnar Suspension Plasma Spray (SPS) Coatings by Pre-Oxidation of the CoNiCrAlY Bondcoat. *Coatings* **2023**, *13*, 1575. https://doi.org/10.3390/coatings13091575

Academic Editor: Alessandro Patelli

Received: 31 July 2023
Revised: 14 August 2023
Accepted: 7 September 2023
Published: 9 September 2023

Copyright: © 2023 by the authors. Licensee MDPI, Basel, Switzerland. This article is an open access article distributed under the terms and conditions of the Creative Commons Attribution (CC BY) license (https://creativecommons.org/licenses/by/4.0/).

1. Introduction

Ecological and economic aspects are becoming increasingly important in the field of turbine development, encompassing both stationary and aircraft turbines. Recent research efforts have been primarily focused on enhancing the efficiency of turbines [1]. However, this objective can only be accomplished by elevating the turbine inlet temperature, which, in turn, imposes higher stress and faster degradation on the utilized materials and reduces the lifespan of components [2,3]. Consequently, it is essential to devise novel materials and material combinations, as well as enhanced processing for TBCs, that can withstand the increased thermal and mechanical loads, thus enabling extended lifetimes even at elevated turbine temperatures.

There are several potential causes for the failure of thermal barrier coatings. High temperatures during turbine operation cause stresses arising from monoclinic phase transformations [4] and sintering processes [5] in the yttria-partially-stabilized zirconia (YSZ). Additionally, the different thermal expansion coefficients [6] of the metallic and ceramic layers and the growth of the thermally grown oxide (TGO) layer on the bondcoat [6,7] can introduce stresses [8]. The growth of the TGO generates radial compressive stresses in the topcoat of the valleys of the bondcoat after cooling, which are converted to tensile stresses through stress inversion once the TGO reaches a critical thickness [9]. The presence of porosity in the valleys of SPS coatings is believed to result in lower compressive stresses.

Consequently, cracks initiated by tensile stresses on the roughness peaks can readily propagate towards regions characterized by decreased compressive stress levels [10]. One possible approach to mitigate these issues is pre-oxidation, which can accelerate the time to stress inversion and prevent crack formation on the roughness peaks by transitioning from tensile to compressive stresses (cf. Figure 1). Pre-oxidation of the bondcoat offers the opportunity to control the growth of the TGO while simultaneously reducing stresses in the topcoat. Depending on the chosen temperature and duration of the heat treatment for pre-oxidation, different phases are formed in the TGO. Studies have indicated that a slow and uniform growth of the TGO achieved at moderate temperatures (<1300 °C) and short dwell times, can prevent the formation of spinels and primarily promote the formation of Al_2O_3 [11]. The growth of the TGO exhibits a parabolic or cubic behavior, with higher growth rates occurring especially at the initial stages of oxidation [8,12].

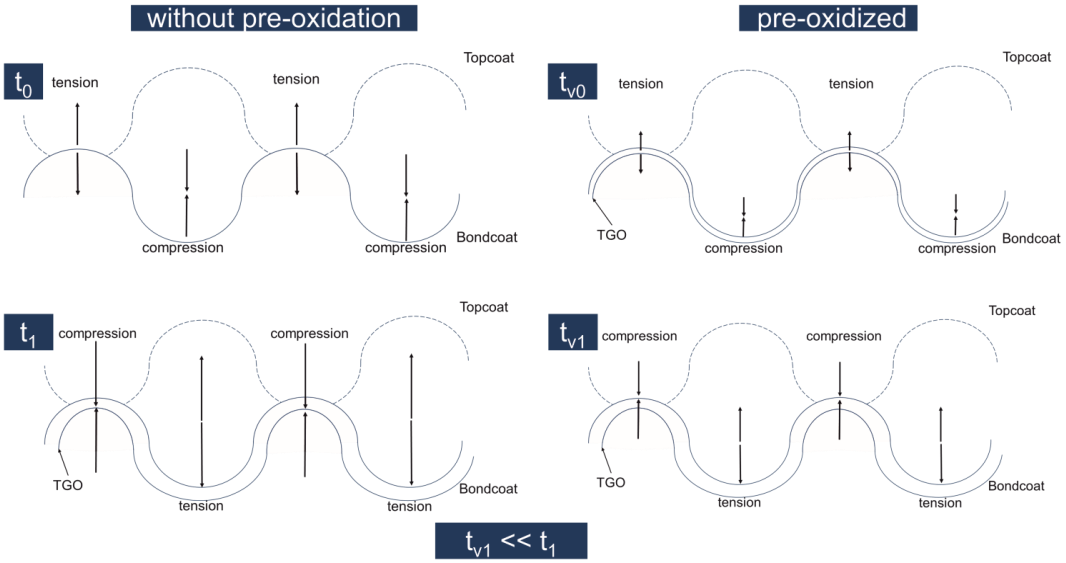


Figure 1. Tensile and compressive stresses in the TGO after cooling from a stress-free high-temperature state. The stress depends on time in a TBC with pre-oxidation of the bondcoat in argon and without pre-oxidation.

Previous research has investigated the utilization of oxide-dispersion-strengthened (ODS) coatings to adjust the coefficient of thermal expansion [13]. The purpose of employing such systems is to compensate for the mismatch of the CTE between bondcoat (about 15×10^{-6}/K) and topcoat (10–11 $\times 10^{-6}$/K) thereby reducing local out-of-plane stresses within the TBC system and enhancing its lifetime. In a conventional thermal barrier coating system, the disparate CTEs affect the extent of expansion and contraction of the materials during the heating and cooling phases of the turbine. During the cooling phase, the metallic layer contracts at a faster rate than the ceramic layer. Assuming that stress relaxation leads to a stress-free state at high temperatures, the ceramic layer experiences compressive stress in the in-plane direction, while tensile stress is induced in the out-of-plane direction [14]. Prolonged thermal cycling of the specimens results in a constant alternation of tensile and compressive stresses in the coating, which promote crack growth and crack propagation, ultimately leading to TBC failure. Past studies have demonstrated that the use of ODS coatings can extend the lifetime of columnar TBCs [15]. The coatings are composed of CoNiCrAlY powder and Al_2O_3. Depending on the oxide powder content, different CTEs are obtained [13]. Proportions below 10 wt.% have been shown to enhance TBC lifetime. Higher proportions of Al_2O_3 in the ODS coating can further minimize the CTE mismatch; however, this may compromise oxidation resistance and subsequently reduce TBC lifetime due to increased oxygen diffusion into the coating [15].

This study focuses on the production and investigation of new coating systems that are intended to extend the lifetime of columnar thermal barrier coatings. In addition to the use of pre-oxidized bondcoats, ODS coatings with coefficients of thermal expansion (CTEs) higher than the bondcoats were tested for their thermal cycling performance. Furthermore, the impact of various microstructures on the cyclic stability of the TBCs is assessed. A comparison of the different approaches with regard to the improvement of the TBC lifetime is made.

2. Experimental Procedure

Since the microstructure of the topcoat strongly depends on the bondcoat properties, vacuum-plasma-sprayed Amdry 9954 bondcoats were exclusively used in this study. These bondcoats were selected for their surface topography and roughness, which facilitate a high column density of the topcoat [16]. The coatings were deposited onto single-crystal CMSX-4 substrate with a diameter of 30 mm. To enhance adhesion between bondcoat and substrate, the surface roughness of the substrate was increased through grit blasting with F36 Al_2O_3 particles. This preparatory step leads to the formation of a recrystallized zone in the near-surface region of the single-crystalline substrate [17], but is indispensable for insurance of coating quality. Following the grit blasting of the substrates, the button-shaped CMSX-4 substrates were coated with a CoNiCrAlY (Amdry 9954, Oerlikon Metco, Wohlen, Switzerland) bondcoat (thickness: 150 µm) using vacuum plasma spraying (VPS) with an F4 torch (Oerlikon Metco, Germany). Additionally, samples TZ4 and TZ5 (cf. Table 1) were coated with an oxide-dispersion-strengthened bondcoat (cf. Figure 2) consisting of Amdry 9954 and 12.5 wt.% or 17.5 wt.% Al_2O_3 (MARTOXID® MR-70, Martinswerk GmbH, Bergheim, Germany). The production of ODS powder is described elsewhere [13]. To facilitate the combined diffusion bonding and bondcoat pre-oxidation, the as-sprayed bondcoats of samples TZ1 to TZ5 (cf. Table 1) were subjected to heat treatment in an argon (99.999% purity) atmosphere at 1 atm. The heat treatment conditions involved 2 h at 1140 °C followed by 16 h at 870 °C. In contrast, sample TZ6 (cf. Table 1) underwent conventional heat treatment in a non-oxidizing atmosphere under vacuum conditions (10^{-3} Pa) at a similar temperature and dwell time. After the heat treatment process, the columnar topcoat was deposited onto the samples. For the production of columnar suspension-plasma-sprayed (SPS) thermal barrier coatings, ethanol-based yttria-stabilized zirconia (YSZ) suspensions (AuerCoat®, Treibacher Industrie AG, Althofen, Austria) were utilized as the feedstock material. The suspensions had different solid contents of 25 wt.% and 40 wt.% and varying average particle sizes, with d_{50} values of 200 nm and 500 nm. The SPS process was performed with the Mettech Axial III torch (Northwest Mettech Corp., Surrey, BC, Canada) producing columnar coatings. The spray distance was set at 70 mm, while the robot speed was maintained at 1000 mm/s. The plasma gas power was adjusted to either 105 or 120 kW. The suspension was conveyed with a feeding system (NanoFeed 350, Northwest Mettech Corp., Canada) where the suspension was transported from a container to the torch via peristaltic pump at a rate of 50 mL/min. To prevent line clogging or feedstock agglomeration, the suspension was circulated outside the coating process duration.

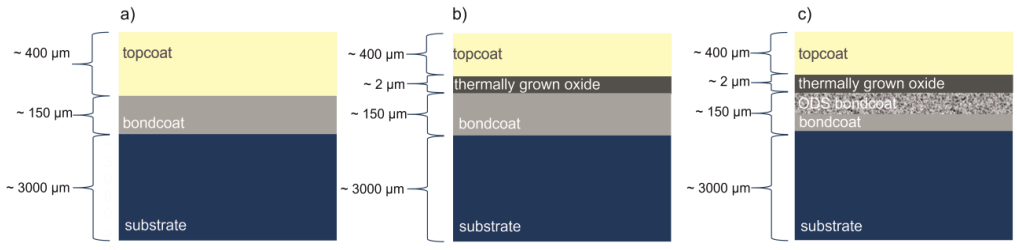


Figure 2. Structure of TBCs without pre-oxidized TGO (**a**), with pre-oxidation of bondcoat and TGO growth (**b**) and with ODS bondcoat (**c**).

Table 1. Spray parameters for deposition of SPS topcoats and structure of the coating system.

Coating	Suspension [wt.%]	$Ar/N_2/H_2$ [%] Power [kW]	TBC System	Heat Treatment
TZ1	40	75/10/15 105	BC/TGO/TC	argon
TZ2	25	75/10/15 105	BC/TGO/TC	argon
TZ3	40	65/10/25 120	BC/TGO/TC	argon
TZ4	25	75/10/15 105	BC/17,5ODS/TGO/TC	argon
TZ5	25	75/10/15 105	BC/12,5ODS/TGO/TC	argon
TZ6	25	75/10/15 105	BC/TC	vacuum

Depending on the selected SPS parameters, different microstructures can be obtained. It has already been reported that particle size distribution of suspensions as well as feed rates and solids load have a strong effect on coating porosity and column formation. To evaluate the effect of different microstructures and bondcoat pre-treatments on TBC lifetime, coatings were produced using different suspensions. Table 1 provides an overview of the spray parameters and the investigated coating systems.

To investigate the failure behavior of the aforementioned TBC systems, thermal cycle tests were conducted using burner rigs. In this procedure, a flame was positioned on the surface of the TBC while the backside was cooled to achieve a desired substrate temperature. The resulting thermal gradient was maintained for 5 min, followed by a single cooling step applied to both the backside and frontside for 2 min [18]. The surface temperature of the TBC was set to 1400 °C, while the substrate temperature was set to 1050 °C. Both temperatures were continuously monitored throughout the cycling of the samples. By considering an emissivity value of 1 for the YSZ coating, the temperature of the bondcoat can be calculated using the measured temperatures and the coating thickness.

The burner rigs are utilized to apply a thermal gradient, where the temperature decreases from the topcoat to the substrate. This setup helps to reduce the impact of coefficient of thermal expansion (CTE) mismatch compared to isothermal cycle tests. However, it is important to note that this method still provides a more realistic simulation of conditions experienced in an actual turbine, especially showing harsh transient phases [19].

To characterize the phases present in the as-sprayed bondcoat, X-ray diffraction (XRD, Empyrean, Malvern Panalytical B.V., Almelo, The Netherlands) using CuKα radiation and Raman spectroscopy were carried out. The XRD measurements covered a 2θ range of 10–90° with a step size of 0.026° and a counting time of 250 s/step. A 255-channel linear PIXcel detector was utilized for data collection. Rietveld analysis of the XRD data was performed using TOPAS software V 4.2 (Bruker Corporation, Billerica, MA, USA). Raman spectroscopy mapping (inVia™ Qontor®, Renishaw GmbH, Pliezhausen, Germany) was performed with a 532 nm laser (~2.5 mW) and a 2400 L mm^{-1} grating. The spectra were collected with a step size of (x, y) = (1 µm, 1 µm) over an area of 80 µm × 40 µm with a total number of 3321 spectra and a measuring time of 1 s per spectrum. The spectra were processed, including cosmic ray removal, truncation, background subtraction and normalization, and afterwards the multiple spectra were averaged to a single spectrum. After component failure, the samples were embedded and prepared by grinding and polishing. Afterwards the sample microstructures were analyzed using scanning electron microscopy (SEM, TM3000, Hitachi, Tokyo, Japan and Gemini SEM 450, Carl Zeiss NTS GmbH, Oberkochen, Germany), the latter equipped with an Ultim® Max 170 EDS detector

(Oxford Instruments NanoAnalysis, Abingdon, UK). To determine the porosity of the coatings, image analysis was performed using the FIJI software 2.14.0 (FIJI) [20].

3. Results and Discussion

3.1. Phase Characterization

XRD analysis was performed to determine the phase composition of the formed oxide layer on the bondcoat surface after heat treatment. To verify controlled oxidation during heat treatments of the material, three different types of samples were analyzed (cf. Figure 3). First, to ensure that minor bondcoat oxidation occurred during the VPS deposition process of the bondcoat, an as-sprayed sample was characterized as the reference system for phase analysis. The surface of the reference sample consisted solely of metal phases derived from the elements present in the bondcoat powder. The bondcoat powder used in this study was cobalt-based, which accounted for the predominant phase composition of the as-sprayed bondcoat, reflected in the comparably higher intensity of the peaks at a 2θ angles of 51°, 75° and 82°, as determined by Rietveld analysis. The phase composition of the heat-treated samples demonstrated the formation of α-alumina during the heat treatment process, under both argon and vacuum conditions (2θ angle of 26°, 35°, 58°, 66° and 68°). However, the proportion of alumina in the argon heat-treated samples is significantly higher, showing higher peak intensities compared to vacuum heat-treated samples. The third phase detected is the AlCo ß-phase (2θ angle of 31°, 44° and 65°).

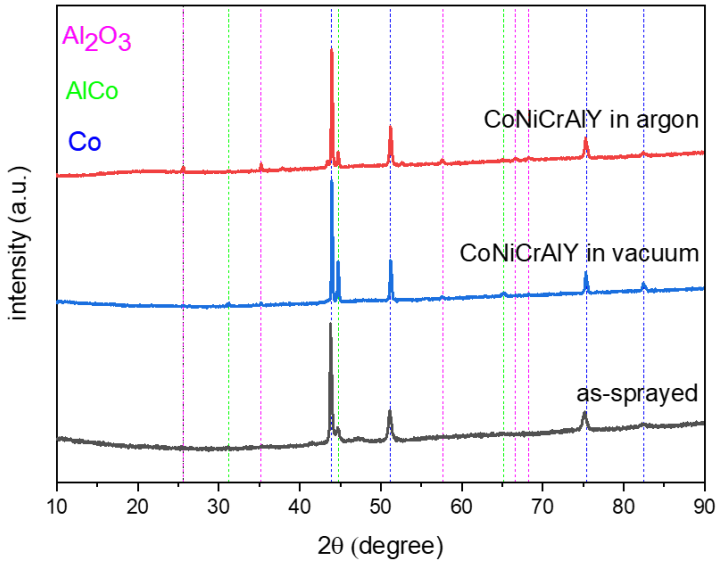


Figure 3. XRD patterns of heat-treated bondcoats in argon and vacuum showing the formation of Al_2O_3 and the reference pattern of the as-sprayed bondcoat.

To further analyze the elemental distribution of the thermally grown oxide and bondcoat, EDS measurements were conducted to clarify in more detail the composition of the approximately 1 µm thick oxide layer (cf. Figure 4). For this purpose, SEM images of the microstructure were captured to investigate the elemental distribution within the different layers of the TBC via EDS analysis. The Amdry 9954 bondcoat typically exhibits a two-phase microstructure [21], comprising the β-(Co,Ni)Al phase and γ-Ni/Co phase. The EDS mappings revealed the presence of Ni- and Al-rich phases (β-phase) as well as Cr-, Co- and Ni-rich (γ-phase) regions within the Amdry 9954 bondcoat. The topcoat, made of YSZ, consists of Zr, Y and O. For the oxide layer which is located between the topcoat and bondcoat, the EDS measurements show that it consists primarily of alumina, with yttrium-rich precipitates. The XRD measurements of the bondcoat only detected Al_2O_3 phases, due to low concentrations of the yttrium-containing phases (below the XRD detection limit of 1–2 wt.% [22]) during the oxidation process.

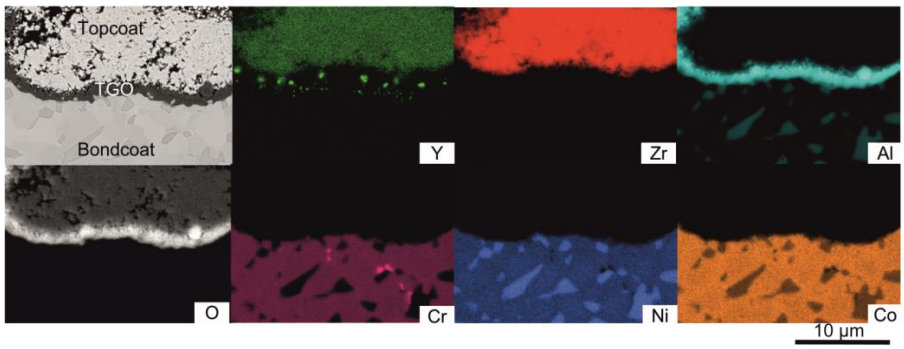


Figure 4. EDS mapping of a pre-oxidized bondcoat in argon with TGO formation.

To investigate the Y-containing phases present in the oxide layer, Raman spectroscopy was employed to analyze the composition of the TGO. Initially, the CoNiCrAlY bondcoat surface was examined without any oxide phases detected, indicating its metallic nature prior to the heat treatment. This absence of Raman signals can be attributed to the low or even absent Raman signal of metals. However, after an 18 h heat treatment at elevated temperatures in either vacuum or argon, the CoNiCrAlY alloy surface exhibited multiple Raman signals, indicating an oxidation process (cf. Figure 5a). Remarkably, the samples treated in argon and vacuum showed similar characteristics with only minor differences: multiple lines at 201, 236, 276, 308, 318, 335, 335, 387, 419, 435, 480, 512, 525, 560, 573, 604, 652, 698, 756, 781, 810, 836 and 910 cm^{-1} were found. For the detection of the signals, a $YAlO_3$ powder reference was measured (Figure 5b), exhibiting a highly similar spectrum. This indicates that $YAlO_3$ is likely one of the oxide phases formed during the oxidation process on the CoNiCrAlY surface [23]. However, in quantities below the detection limit of XRD, some differences were observed between the oxide layer spectra and the reference spectra, suggesting variations in their composition or the occurrence of stresses. It is possible that the Y content in the oxide layer is lower than in the stoichiometric $YAlO_3$ reference sample, resulting in the slight differences in the Raman spectra. In addition to the $YAlO_3$ signals, the oxide layer also reveals a signal at 318 cm^{-1}, which is likely attributed to the prominent Raman signal of Al_2O_3 (Figure 5b) [24]. Although the XRD and EDS results indicate that the Al_2O_3 Raman phase constitutes the majority of the oxide layer, the Al_2O_3 signals of the Raman analysis were relatively weak in intensity compared to the $YAlO_3$ signals. This behavior could be explained by the higher Raman activity of the $YAlO_3$ phase compared to the Al_2O_3 phase. To confirm this assumption, $YAlO_3$ and Al_2O_3 powders were separately measured under identical parameters (Figure 5b), revealing $YAlO_3$ signals 16 times higher in intensity than the signals of the Al_2O_3 phase.

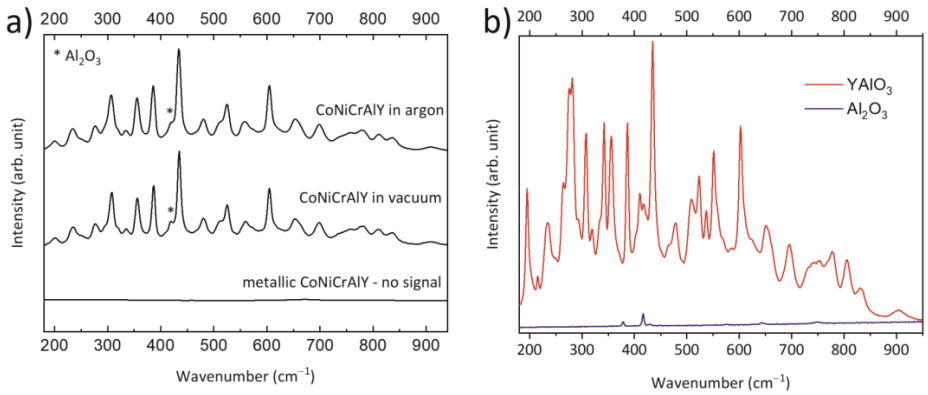


Figure 5. Raman spectra of (**a**) untreated and heat-treated bondcoats in vacuum and argon; (**b**) Al_2O_3 and $YAlO_3$ references measured with the same parameters without any normalization.

Based on these results, in combination with the XRD and EDS findings, it can be concluded that the oxide layer primarily consists of Al_2O_3 with inclusions of Y, forming a $YAlO_3$ phase that is likely not completely stoichiometric.

Based on the comprehensive analysis conducted on the phases and elements in the oxide layer, it can be confidently concluded that heat treating the CoNiCrAlY bondcoats in an argon atmosphere results in the uniform growth of a thermally grown oxide (TGO) layer predominantly composed of dense Al_2O_3, along with yttrium aluminate precipitates. It should be noted that the concentration of yttrium aluminate precipitates might be too low to be detected using X-ray diffraction (XRD) techniques. Raman spectroscopy detected the presence of the phase, particularly enriched near the surface, which aligns with the findings from energy-dispersive X-ray spectroscopy (EDS) analysis. The results indicate that the heat treatment in argon promotes the formation of a well-defined oxide layer. In contrast, heat treating the bondcoats in a vacuum environment leads to the growth of low-concentration oxides on the surface. These oxides form a layer that is too thin to be resolved in the scanning electron microscope (SEM) cross-sections. The results obtained from both energy-dispersive X-ray spectroscopy (EDS) and Raman spectroscopy align with regards to the oxidation of the different heat-treated substrates. It is evident from both measurement methods that the as-sprayed samples (prior to heat treatment) did not exhibit any oxide formation.

Depending on the growth condition of the TGO layer, different types of oxides can be formed [25]. The desired composition for the TGO is solely α-Al_2O_3. The growth rate and composition depend on the oxygen content in the surrounding environment during heat treatment and the dominant growth mechanism. In sufficient oxygen-containing atmospheres, TGO formation proceeds within a short period compared to atmospheres with lower oxygen content. However, extended exposure to high oxygen levels can lead to the formation of undesirable mixed oxides and spinel compounds over time [26]. This uneven growth of the oxide layer can result in increased stress accumulation within the coating [27], ultimately reducing the lifetime of the thermal barrier coating.

3.2. Thermal Cycling Results

The SPS process parameters have a significant impact on both the microstructure and mechanical properties of the coating, as highlighted in the study by Joeris et al. [16]. To investigate the specific areas where the thermal barrier coatings fail after thermal cycling, cross-sectional scanning electron microscopy (SEM) images were captured and analyzed. Additionally, photographs of the failed substrates were included for reference.

Figure 6 illustrates the cross-section of sample TZ1, which underwent pre-oxidation in an argon environment, leading to the formation of an intermediate oxide layer at the interface between the topcoat and bondcoat. Following thermal cycling, the delamination of the specimen occurred primarily at the edge regions of the topcoat, resulting in "blue" failure on the delaminated surface. Blue failure indicates failure at the oxide layer. The crack propagation is observed along the interface between the thermally grown oxide (TGO) layer and the topcoat, occasionally leading to adhesions of the topcoat within the valleys of the TGO. Furthermore, in certain regions, the crack extends through the TGO layer.

The failure behavior is consistent among specimens produced using a lower solids content of 25 wt.% (cf. Figure 7, TZ2). The YSZ coating on this sample exhibits a columnar microstructure. The porosity decreased from 18.8% to 9% compared to sample TZ1 using a diluted suspension. After thermal cycling, delamination of the coating is observed at the center of the specimen surface, accompanied by both "white" and "blue" failure modes, where "white" failure indicates a failure in the ceramic layer. The thermally grown oxide (TGO) layer, formed between the bondcoat and topcoat, is visible as a dark intermediate layer. The crack formed in the TBC runs along the TGO/topcoat interface, with residual fragments of the topcoat being trapped within the valleys of the bondcoat rather than spalling off.

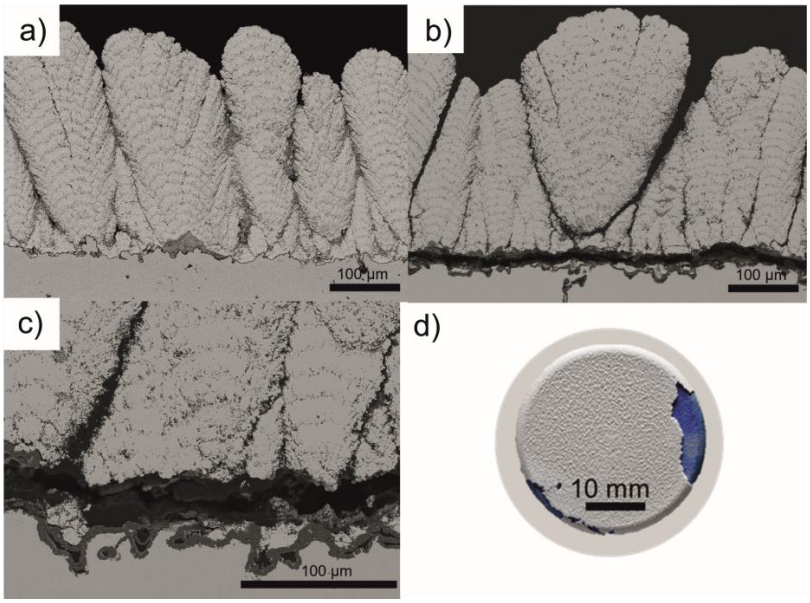


Figure 6. SEM images of sample TZ1 in the as-sprayed state (**a**), after thermal cycling test (**b**,**c**) and photograph of the sample's surface (**d**).

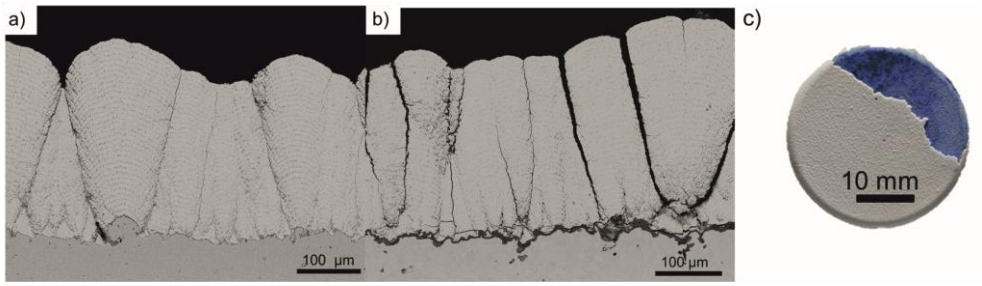


Figure 7. SEM images of sample TZ2 in the as-sprayed state (**a**), after thermal cycling test (**b**) and a photograph of the button-shaped sample surface (**c**).

Sample TZ3 underwent pre-oxidation of the bondcoat in an argon environment and was sprayed with 40 wt.% YSZ suspension (cf. Figure 8). The use of higher power from 105 kW to 120 kW during the SPS process results in increased layer formation within the columns [16], accompanied by a decrease in total porosity from 18.8% (TZ1) to 12.4% (TZ3). Delamination of the surface is observed at the edge region and "blue" failure is evident. The crack propagates along the interface between the thermally grown oxide (TGO) layer and the topcoat, extending through the TGO layer. Minor and irregular ceramic attachments can be observed within the valleys of the TGO layer.

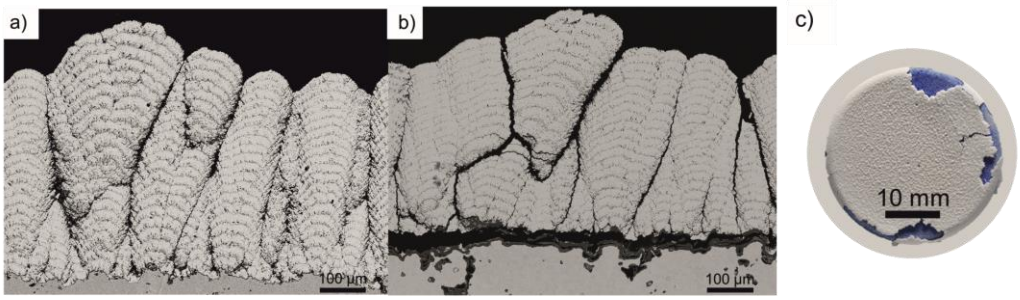


Figure 8. SEM images of sample TZ3 in the as-sprayed state (**a**), cross-section of a failed coating after thermal cycling test (**b**) and a photograph of the button-shaped sample surface (**c**).

A reason for the formation of cracks or delamination of the topcoat can be the monoclinic phase transformations in the YSZ coating. The phase transformation of YSZ from tetragonal (t') to tetragonal (t) and cubic (c) and then to monoclinic (m) [28] can potentially lead to failure of the TBC as the volume change induces stresses and generates cracks [29]. XRD measurements were conducted on the thermally cycled samples (cf. Figure 9) to assess the presence of monoclinic phase peaks at 2θ angles of 25° to 35° (cf. Figure 9a) and at the 2θ range of 73° to 75° (cf. Figure 9b) which, according to Witz et al. [29], are characteristic 2θ ranges for monoclinic (m), tetragonal (t) and cubic (c) phases. The absence of these characteristic peaks in Figure 9 suggests that minor or no significant monoclinic phase transformation has occurred in the samples. Most of the thermally cycled samples still exhibit a tetragonal phase. In sample TZ4 (cf. Figure 9a), the additional peak observed can be attributed to the formation of mixed oxides, such as Co-oxide, resulting from the oxidation of the bondcoat. This analysis was performed in areas where topcoat delamination had taken place. Considering that the monoclinic phase transformation only occurred to a limited extent in the samples, it is unlikely to be the primary cause of their failure.

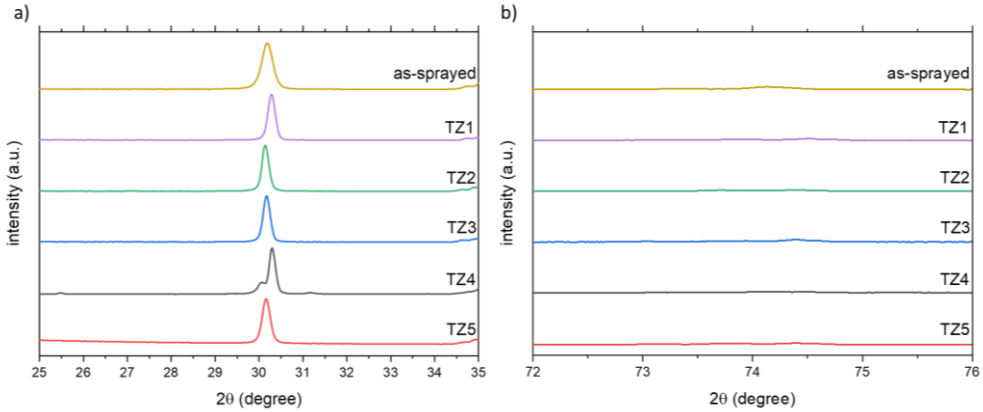


Figure 9. XRD pattern of as-sprayed and thermally cycled samples showing no monoclinic phases after thermal cycling at characteristic 2θ angles of (**a**) 25° to 35° and (**b**) 73° to 75°.

The growth of the TGO can induce stresses and contribute to the failure of the TBC for thick scales. In standard SPS coatings without bondcoat pre-oxidation, failures often occur when the TGO thickness is low (e.g., 2 µm in [30]) during thermal cycling. As the TGO growth kinetics are non-linear, the initial growth of the TGO is significantly faster in non-pre-oxidized samples. Additionally the growth rate and composition of the TGO can depend on oxygen partial pressure in atmosphere [25]. By employing a moderate pre-oxidation technique, the undesirable rapid growth of oxide scales and their detrimental effects on the stress state in the topcoat can be effectively reduced. A high growth rate implies a significant increase in volume within a short period, leading to higher stresses in the TBC. Pre-oxidation can reduce this initial phase and potentially reduce the stress levels. Figure 10 shows the thickness of the TGO layers after pre-oxidation (T0) and after thermal cycling (TZ1–TZ5). The standard deviation of the TGO thickness results from the non-uniform growth of the TGO on the rough bondcoat surface during thermal cycling and, in particular, from damage to the thermal barrier layer and the resulting faster growth of the TGO in specific regions. However, there is no direct correlation between TGO thickness and cycle time. This might be due to large variations in TGO thickness to the roughness profile, as well as to compositional effects and the corresponding uncertainty in the measurement. However, it is obvious that the TGO thickness is always rather large, at least above 5 µm.

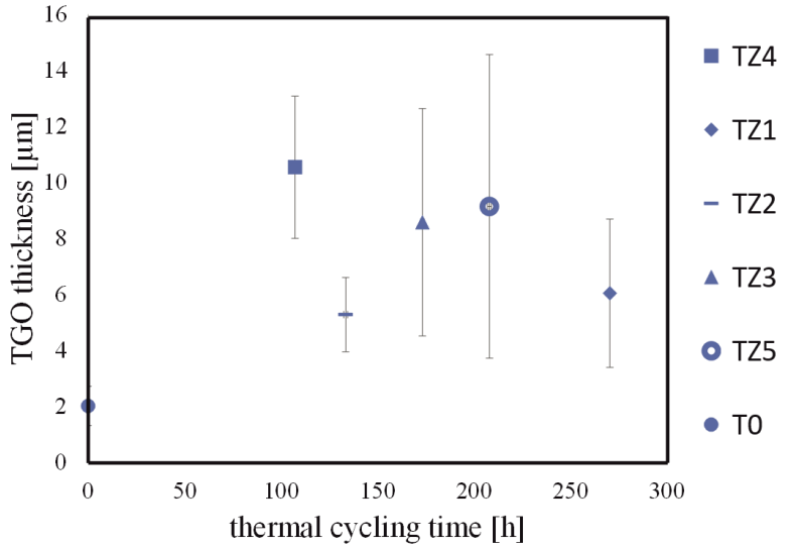


Figure 10. TGO thickness of thermally cycled samples with pre-oxidation in argon.

Typically, APS coatings demonstrate an average thermal cycle resistance of approximately 1000 cycles, while SPS coatings achieve lifetimes of up to 350 cycles [31]. In this study, by pre-oxidizing the bondcoat in argon, cycle resistances of up to 2434 cycles were achieved. Consequently, the lifetimes of SPS coatings not only surpass those of combined layer systems comprising APS/SPS [10] and ODS/SPS [15], but also outperform APS layers [31]. The lowest lifetime observed was 920 cycles for the ODS/SPS sample TZ4. The higher amount of Al_2O_3 lead to large internal oxidation. The 12.5 wt.% sample performed better, however performance improvement was also found in samples with a 10 wt.% addition [13]. The highest lifetime of 2434 cycles (cf. Figure 11, sample TZ1) was achieved by employing a bondcoat pre-oxidation in argon and a 40 wt.% suspension for topcoat deposition, resulting in higher porosity. The ODS/SPS coating systems and coatings that underwent pre-oxidation in argon, produced with a 25 wt.% suspension or a 40 wt.% suspension and high power during spraying, demonstrate cycle resistances ranging from 920 to 1784 cycles, with ODS coatings exhibiting comparatively lower performance than SPS coating without an intermediate ODS layer.

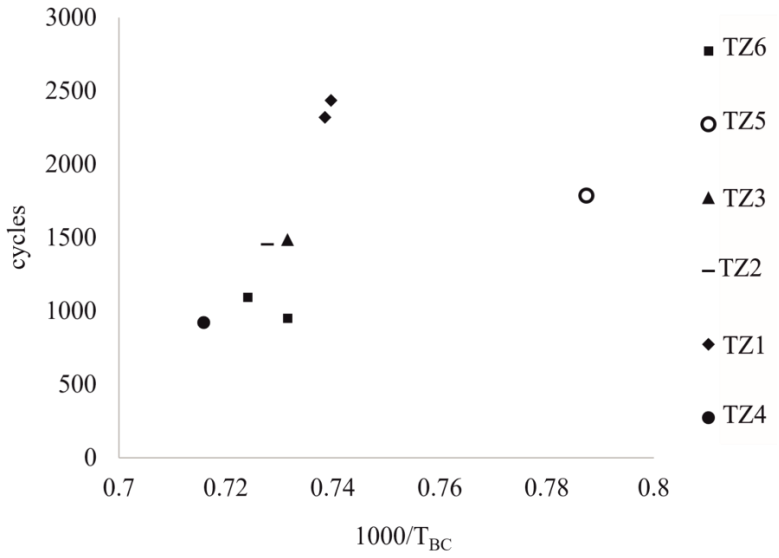


Figure 11. Results of burner rig tests with surface temperature of 1400 °C for SPS TBCs as a function of the reciprocal bondcoat temperature.

The pre-oxidation of the bondcoats in argon has been found to impact both the lifetime and failure mechanism of the TBC. Previous studies have shown that columnar SPS thermal barrier coatings, subjected to standard vacuum bondcoat heat treatment, fail a few microns above the TGO within the topcoat itself [10]. However, with stronger pre-oxidation of the bondcoats in argon, the crack formation during thermal cycling of the TBCs no longer occurs within the topcoat, but instead follows along the TGO/TC interface or within the TGO layer itself. Only small residual fragments of the topcoat remain attached to the bondcoat within the valleys of the TGO. The differing failure mechanisms could be attributed to the growth behavior of the TGO. The parabolic growth of the TGO [8,12] during oxidation results in higher growth rates during the initial stages of oxide formation. Consequently, the volume expansion is more pronounced during this initial phase. When the topcoat is applied to an already pre-formed TGO, the initial stresses and growth-induced stresses within the coating might be reduced.

When comparing a system without pre-oxidation and TGO growth and a system with pre-oxidation (cf. Figure 1), there could be differences in the time between the start of thermal cycling (t0) and the occurrence of stress reversal due to TGO growth (t1, tv1). In the case of pre-oxidation, the presence of an already-formed TGO might lead to an earlier stress reversal (tv1) compared to a non-pre-oxidized sample (t1). As a result, it is possible that cracks cannot form and propagate on the roughness peaks because the time to stress reversal is shortened and the initial stress level is reduced by pre-oxidation. The reduction in the time to stress reversal might contribute to the longer lifetimes of the specimens. In the pre-oxidized samples, the cracks tend to form in the valleys and propagate from there as these areas are under tensile stress. This failure pattern is similar to the findings of Renusch et al. [32], who demonstrated that thermal aging caused by TGO growth and sintering of YSZ as well as Al depletion in the bondcoat contribute to specimen failure. In both cases, crack growth occurs at the TGO/TC interface or within the TGO itself [32]. The growth of the TGO can induce cracks at the edge regions of the roughness peaks due to the development of high tensile stresses (parallel to the interface) caused by the volume expansion of the TGO [33]. These cracks typically run along the TGO/TC interface when the TGO reaches a critical thickness at which coating failure occurs [6]. As the specimen cools down, the cracks can propagate and connect with each other.

4. Summary and Conclusions

The pre-oxidation of bondcoats in argon prior to the deposition of thermal barrier coatings (TBCs) has proven to be beneficial in terms of extending the lifetime of columnar suspension-plasma-sprayed coatings and altering the failure mechanism. By promoting the growth of the TGO before thermal cycling, the stress distribution within the coating system is modified, resulting in a shift of crack formation and propagation. Cracks tend to occur in the valleys of the TGO, and the topcoat remains partially attached to the TGO/BC after spallation of the coating.

This change in failure behavior might be attributed to the reduction of initial stresses and growth stresses induced by pre-oxidation. The presence of an already-formed TGO during thermal cycling might affect the stress reversal process and potentially prevent crack initiation on roughness peaks. Consequently, the lifetimes of pre-oxidized TBCs are extended compared to non-pre-oxidized counterparts.

These findings highlight the importance of understanding the influence of pre-oxidation and TGO growth on the mechanical behavior of TBCs. Further research in this area could provide insights into optimizing coating designs and process parameters to enhance the performance and durability of columnar SPS coatings or of thermal barrier coatings in general.

Author Contributions: J.J.: Conceptualization, investigation, methodology, writing—original draft; W.S.S.: Investigation and writing; S.U.: Investigation and editing; Y.J.S.: Investigation and editing; D.S.: Investigation and editing; O.G.: Supervision and editing; R.V.: Supervision and editing. All authors have read and agreed to the published version of the manuscript.

Funding: This work was funded within the project T5 in SFB/TR 103 "From Atoms to Turbine Blades"by the German research Foundation (DFG), project nr. 190389738.

Data Availability Statement: Data are contained within the article.

Acknowledgments: The first author would like to thank her colleagues Emine Bakan and Simon Schöler for support in the interpretation and discussion of the results. Further thanks go to Frank Kurze, Ralf Laufs and Karl-Heinz Rauwald for their support in the production of the TBCs and to Martin Tandler for monitoring of the burner rig tests.

Conflicts of Interest: The authors declare no conflict of interest.

References

1. Stöver, D.; Funke, C. Directions of the Development of Thermal Barrier Coatings in Energy Applications. *J. Mater. Process. Technol.* **1999**, *93*, 195–202. [CrossRef]
2. Carter, T.J. Common Failures in Gas Turbine Blades. *Eng. Fail. Anal.* **2005**, *12*, 237–247. [CrossRef]
3. Chang, J.C.; Yun, Y.H.; Choi, C.; Kim, J.C. Failure Analysis of Gas Turbine Buckets. *Eng. Fail. Anal.* **2003**, *10*, 559–567. [CrossRef]
4. Chevalier, J.; Gremillard, L.; Virkar, A.V.; Clarke, D.R. The tetragonal-monoclinic transformation in zirconia: Lessons learned and future trends. *J. Am. Ceram. Soc.* **2009**, *92*, 1901–1920. [CrossRef]
5. Thompson, J.A.; Clyne, T.W. The Stiffness of Plasma Sprayed Zirconia Top Coats in TBCS. *Therm. Spray 1999 Proc. United Therm. Spray Conf.* **1999**, *83836*, 835–840. [CrossRef]
6. Rabiei, A.; Evans, G.A. Failure Mechanisms Associated with the Thermally Grown Oxide in Plasma-Sprayed Thermal Barrier Coatings Author Links Open Overlay PanelARabieiaA.GEvansb. *Acta Mater.* **2000**, *48*, 3963–3976. [CrossRef]
7. Miller, R.A. Current Status of Thermal Barrier Coatings—An Overview. *Surf. Coatings Technol.* **1987**, *30*, 1–11. [CrossRef]
8. Liu, X.; Wang, T.; Li, C.; Zheng, Z.; Li, Q. Microstructural Evolution and Growth Kinetics of Thermally Grown Oxides in Plasma Sprayed Thermal Barrier Coatings. *Prog. Nat. Sci. Mater. Int.* **2016**, *26*, 103–111. [CrossRef]
9. Gupta, M.; Eriksson, R.; Sand, U.; Nylén, P.A. Diffusion-based oxide layer growth model using real interface roughness in thermal barrier coatings for lifetime assessment. *Surf. Coat. Technol.* **2015**, *271*, 181–191. [CrossRef]
10. Zhou, D.; Mack, D.E.; Gerald, P.; Guillon, O.; Vaßen, R. Architecture Designs for Extending Thermal Cycling Lifetime of Suspension Plasma Sprayed Thermal Barrier Coatings. *Ceram. Int.* **2019**, *45*, 18471–18479. [CrossRef]
11. Chang, W.L.E.; Wu, B.C.; Chao, C.H. Effects of Bond Coat Preoxidation on the Properties of ZrO_2-8wt.% Y_2O_3/Ni-22Cr-10Al-1Y Thermal-Barrier Coatings. *Oxid. Met.* **1991**, *36*, 221–238. [CrossRef]
12. Niranatlumpong, P.; Ponton, C.B.; Evans, H.E. Failure of Protective Oxides on Plasma-Sprayed NiCrAlY Overlay Coatings. *Oxid. Met.* **2000**, *53*, 241–258. [CrossRef]
13. Vorkötter, C.; Hagen, S.P.; Pintsuk, G.; Mack, D.E.; Virtanen, S.; Guillon, O.; Vaßen, R. Oxide Dispersion Strengthened Bond Coats with Higher Alumina Content: Oxidation Resistance and Influence on Thermal Barrier Coating Lifetime. *Oxid. Met.* **2019**, *92*, 167–194. [CrossRef]
14. Teixeira, V.; Andritschky, M.; Fischer, W.; Buchkremer, H.P.; Stöver, D. Analysis of Residual Stresses in Thermal Barrier Coatings. *J. Mater. Process. Technol.* **1999**, *92–93*, 209–216. [CrossRef]
15. Vorkötter, C.; Mack, D.E.; Zhou, D.; Guillon, O.; Vaßen, R. Effect of Low-CTE Oxide-Dispersion-Strengthened Bond Coats on Columnar-Structured YSZ Coatings. *Coatings* **2022**, *12*, 396. [CrossRef]
16. Joeris, J.; Tiwari, A.; Brinckmann, S.; Kurze, F.; Guillon, O.; Vaßen, R. Evaluation of Major Factors Influencing the TBC Topcoat Formation in Axial Suspension Plasma Spraying (SPS). *Int. J. Appl. Ceram Technol.* **2022**, *20*, 884–895. [CrossRef]
17. Kalfhaus, T. *Entwicklung von Reparaturmethoden Für Nickel-Superlegierungen Mittels Thermischer Spritzverfahren*; [Development of Repair Methods for Nickel Superalloys Using Thermal Spray Techniques, Ph.D thesis]; Werkstoffsynthese und Herstellungsverfahren: Jülich, Germany, 2019.
18. Feist, J.; Sollazzo, P.Y.; Pilgrim, C.; Nicholls, J. Operation of a Burner Rig for Thermal Gradient Cycling of Thermal Barrier Coatings. In Proceedings of the ASME Turbo Expo 2014: Turbine Technical Conference and Exposition, Düsseldorf, Germany, 16–20 June 2014. [CrossRef]
19. Sundaram, S.; Lipkin, D.M.; Johnson, C.A.; Hutchinson, J.W. The influence of transient thermal gradients and substrate constraint on delamination of thermal barrier coatings. *J. Appl. Mech.* **2013**, *80*, 0110022. [CrossRef]
20. Schindelin, J.; Arganda-Carreras, I.; Frise, E.; Kaynig, V.; Longair, M.; Pietzsch, T.; Preibisch, S.; Rueden, C.; Saalfeld, S.; Schmid, B.; et al. Fiji: An Open-Source Platform for Biological-Image Analysis. *Nat. Methods* **2012**, *9*, 676–682.
21. Saeidi, S.; Voisey, K.T.; McCartney, D.G. Mechanical Properties and Microstructure of VPS and HVOF CoNiCrAlY Coatings. *J. Therm Spray Tech.* **2011**, *20*, 1231–1243. [CrossRef]
22. Surana, R.; Suryanarayanan, R. Quantitation of Crystallinity in Substantially Amorphous Pharmaceuticals and Study of Crystallization Kinetics by X-Ray Powder Diffractometry. *Powder Diffr.* **2000**, *15*, 2–6. [CrossRef]
23. Hernández-Rodríguez, M.A.; Monteseguro, V.; Lozano-Gorrín, A.D.; Manjón, F.J.; González-Platas, J.; Rodríguez-Hernández, P.; Muñoz, A.; Lavín, V.; Martín, I.R.; Rodríguez-Mendoza, U.R. Structural, Vibrational, and Elastic Properties of Yttrium Orthoaluminate Nanoperovskite at High Pressures. *J. Phys. Chem. C* **2017**, *121*, 15353–15367. [CrossRef]

24. Thapa, J.; Liu, B.; Woodruff, S.D.; Chorpening, B.T.; Buric, M.P. Raman Scattering in Single-Crystal Sapphire at Elevated Temperatures. *Appl. Opt.* **2017**, *56*, 8598–8606.
25. Nijdam, T.J.; Jeurgens, L.P.H.; Chen, J.H.; Sloof, W.G. On the Microstructure of the Initial Oxide Grown by Controlled Annealing and Oxidation on a NiCoCrAlY Bond Coating. *Oxid. Met.* **2005**, *64*, 355–377. [CrossRef]
26. Nijdam, T.J.; Sloof, W.G. Combined Pre-Annealing and Pre-Oxidation Treatment for the Processing of Thermal Barrier Coatings on NiCoCrAlY Bond Coatings. *Surf. Coat. Technol.* **2006**, *201*, 3894–3900. [CrossRef]
27. Zhou, Z.J.; Li, C.P.; Chen, G.F.; Hua, X.; Li, Y. Thermomechanical and Thermal Gradient Mechanical Fatigue Lifetime of Thermal Barrier Coating Systems. *Mater. Sci. Forum* **2017**, *898 MSF*, 1524–1531. [CrossRef]
28. Miller, R.A.; Smialek, J.L.; Garlick, R.G. Phase Stability in Plasma-Sprayed, Partially Stabilized Zirconia-Yttria. *Adv. Ceram.* **1981**, *3*, 241–253.
29. Witz, G.; Shklover, V.; Steurer, W.; Bachegowda, S.; Bossmann, H.P. Phase Evolution in Yttria-Stabilized Zirconia Thermal Barrier Coatings Studied by Rietveld Refinement of X-Ray Powder Diffraction Patterns. *J. Am. Ceram. Soc.* **2007**, *90*, 2935–2940. [CrossRef]
30. Zhou, D.; Guillon, O.; Vaßen, R. Development of YSZ Thermal Barrier Coatings Using Axial Suspension Plasma Spraying. *Coatings* **2017**, *7*, 120. [CrossRef]
31. Vaßen, R.; Bakan, E.; Mack, D.E.; Guillon, O. A Perspective on Thermally Sprayed Thermal Barrier Coatings: Current Status and Trends. *J. Therm. Spray Technol.* **2022**, *31*, 685–698. [CrossRef]
32. Renusch, D.; Schorr, M.; Schütze, M. The Role That Bond Coat Depletion of Aluminum Has on the Lifetime of APS-TBC under Oxidizing Conditions. *Mater. Corros.* **2008**, *59*, 547–555. [CrossRef]
33. Evans, H.E. Oxidation Failure of TBC Systems: An Assessment of Mechanisms. *Surf. Coat. Technol.* **2011**, *206*, 1512–1521. [CrossRef]

Disclaimer/Publisher's Note: The statements, opinions and data contained in all publications are solely those of the individual author(s) and contributor(s) and not of MDPI and/or the editor(s). MDPI and/or the editor(s) disclaim responsibility for any injury to people or property resulting from any ideas, methods, instructions or products referred to in the content.